Calcium binding and allosteric signaling mechanisms for the sarcoplasmic reticulum Ca^{2+} ATPase

Peter M. Kekenes-Huskey,[1*†] Vincent T. Metzger,[2,†] Barry J. Grant,[3] and J. Andrew McCammon[1,2]

[1]Department of Pharmacology, University of California, San Diego, La Jolla, California 92093

[2]Department of Chemistry and Biochemistry, University of California, San Diego, La Jolla, California 92093

[3]Department of Computational Medicine and Bioinformatics, University of Michigan, Ann Arbor, Michigan 48109

Received 8 April 2012; Revised 11 July 2012; Accepted 16 July 2012
DOI: 10.1002/pro.2129
Published online 23 July 2012 proteinscience.org

Abstract: The sarcoplasmic reticulum Ca^{2+} ATPase (SERCA) is a membrane-bound pump that utilizes ATP to drive calcium ions from the myocyte cytosol against the higher calcium concentration in the sarcoplasmic reticulum. Conformational transitions associated with Ca^{2+}-binding are important to its catalytic function. We have identified collective motions that partition SERCA crystallographic structures into multiple catalytically-distinct states using principal component analysis. Using Brownian dynamics simulations, we demonstrate the important contribution of surface-exposed, polar residues in the diffusional encounter of Ca^{2+}. Molecular dynamics simulations indicate the role of Glu309 gating in binding Ca^{2+}, as well as subsequent changes in the dynamics of SERCA's cytosolic domains. Together these data provide structural and dynamical insights into a multistep process involving Ca^{2+} binding and catalytic transitions.

Keywords: SERCA; Molecular dynamics; Brownian dynamics; gating; calcium binding

Introduction

The regulation of Ca^{2+} transport by ion channels, pumps, and exchangers is of crucial importance to excitation-contraction coupling in muscle cells. The sarcoplasmic reticulum Ca^{2+} ATPase (SERCA) is a transmembrane (TM) Ca^{2+} pump that transports two Ca^{2+} into the sarcoplasmic reticulum from the cytosol through ATP-dependent conformational transitions. This transport process is characterized by four sequential catalytic states (E1, E1P, E2P, and E2) with each having a distinct conformation.[1] E1 comprise the cytosol-facing, Ca^{2+}-free, and bound states (which we label as E1, E1(Ca), respectively); binding of ATP and subsequent phosphorylation gives rise to the E1P state. E2P is obtained after the E1P state undergoes a transition that exposes bound Ca^{2+} to the SR lumen, after which liberation of the phosphate ion and Ca^{2+} to the lumen yields the E2 state. The pump finally exposes the empty Ca^{2+} ligand binding domain to the cytosol, whereby binding of cytosolic Ca^{2+} completes the cycle and returns SERCA to the E1 state. Understanding the E1→E1P transition thus provides insight into the calcium-dependent aspects of SERCA function during muscle relaxation.

Electron paramagnetic resonance, Forster resonance energy transfer, and X-ray crystallography of the four catalytic states[1–5] of SERCA have identified several components involved in its catalytic activity. These include transmembrane (TM) bundle helices M1

Additional Supporting Information may be found in the online version of this article.

The authors have no conflicts of interest to declare.

†Peter M. Kekenes-Huskey and Vincent T. Metzger contributed equally to this work.

Grant sponsor: NSF; Grant numbers: OCI-0959097 and OCI-1053575; Grant sponsors: National Institutes of Health; National Science Foundation; Howard Hughes Medical Institute; National Biomedical Computation Resource; Center for Theoretical Biological Physics; NSF Supercomputer Centers.

Correspondence to: Peter Kekenes-Huskey, University of California, San Diego, 9500 Gilman Dr., M/C 0365, La Jolla, CA 92093-0365. E-mail: pkekeneshuskey@ucsd.edu

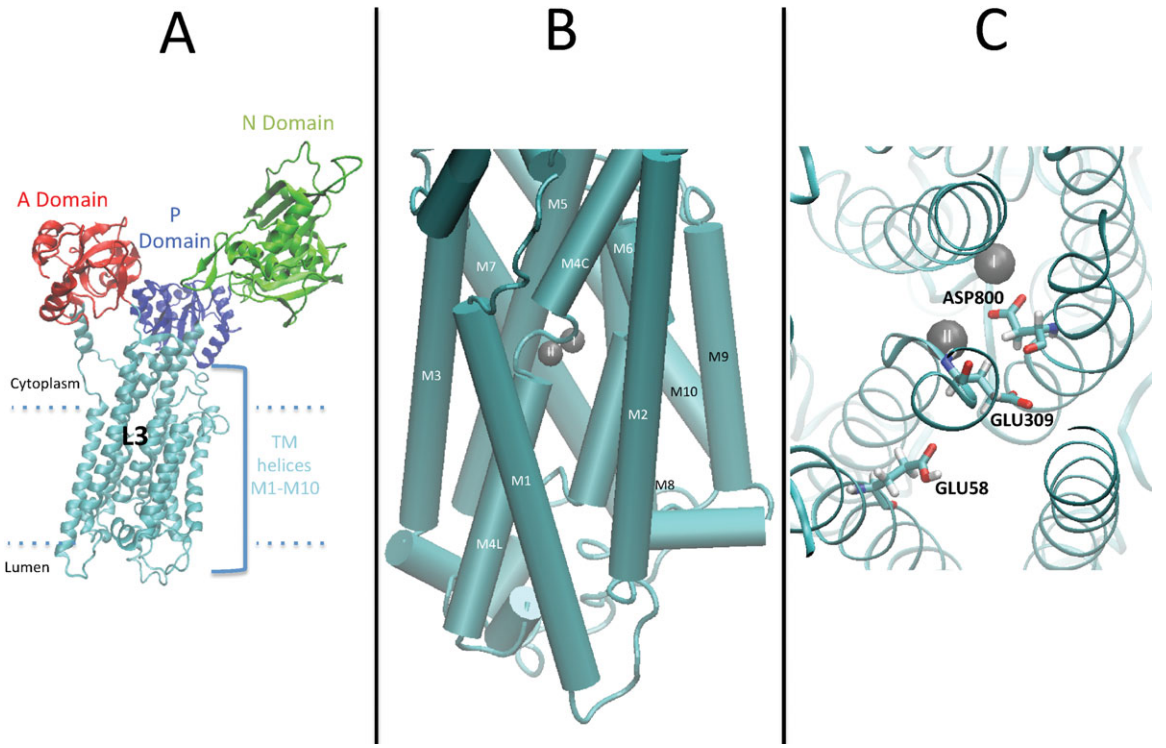

Figure 1. (a) Holo SERCA (PDB ID 1su4) showing the N, A, and P domains as well as the transmembrane helices (teal). (b) Transmembrane region of SERCA with important TM helices labeled. (c) Holo SERCA (PDB ID 1su4) with both Ca^{2+} ions bound (gray) surrounded by several coordinating residues (licorice representation).

to M10, which bind Ca^{2+}, while the cytosolic domains N, P, A are responsible for ATP binding and hydrolysis.[6] (Fig. 1). Upon Ca^{2+} and ATP binding, shifts in M4 and M2, bending of M1, and closing of the A and N cytosolic domains are suggested to promote interchange between E1(Ca) and E1P states[1]; these studies have furthermore identified two Ca^{2+} binding pockets (site I and site II) and residues implicated in Ca^{2+} coordination.

Experiment and simulation have unveiled several key points regarding the cooperative binding of Ca^{2+}. The first calcium is known to bind to site I, which is buried deep with the TM region, and is followed by a second calcium binding to site II, which is closest to the cytoplasm.[7] Binding of calcium to site I increases the calcium affinity of site II, whereupon binding of a second Ca^{2+} is necessary for ATP hydrolysis and continuation of the reaction cycle.[1] Simulations of Ca^{2+} binding to SERCA[8] also indicate that Ca^{2+} binds first at site I, then site II. Bridging site II and the cytoplasm are solvent-exposed acidic residues thought to be involved in Ca^{2+} gating (M4: E309),[9] or recognition (M1: E51, E55, E58, D59[10] and M2: D109[11]) Fig. 1). Residues comprising the cytosolic loops between M6 and M7 (L67) as well as M8 and M9 (L89) have also been implicated in Ca^{2+} binding and ATP turnover and include D813, D815, and D818.[12] However, it remains unclear to what extent these acidic residues are directly involved in Ca^{2+} gating and binding, and moreover, how this binding signal is communicated to the cytosolic domains responsible for ATP hydrolysis.

Molecular dynamics simulations of SERCA have provided substantial insight into the relationship between protein structure and mechanisms of substrate binding, selectivity, and conformational motions. Simulations by Musgaard *et al.*,[18] Huang *et al.*,[8] and Costa *et al.*,[14] have explored possible pathways of Ca^{2+} entry. Specifically, the regions near L67/L89 and M1/M2/M4 have been suggested as predominant pathways for Ca^{2+} binding, which we describe as L1 and L3, respectively (according to the convention in Huang *et al.*), based on MD and solutions of the Poisson-Boltzmann equation. Other simulations have focused on the Ca^{2+} binding domain, thereby, uncovering the importance of particular coordination residues and their protonation states in stabilizing Ca^{2+}.[15,16] Additionally, a recent simulation[17] demonstrated coupling between Ca^{2+} binding and closing of the A and N domains associated with conversion between the E1(Ca) and E1P states. While these studies constitute substantial progress in clarifying the Ca^{2+}-dependent steps of SERCA catalytic activity, the coupling between bulk Ca^{2+} association with SERCA and subsequent catalytic activity has not been well-explored.

We sought to provide a comprehensive and quantitative picture that links Ca^{2+} binding to the protein with important conformational motions, taking into account the role of electrostatic interactions,

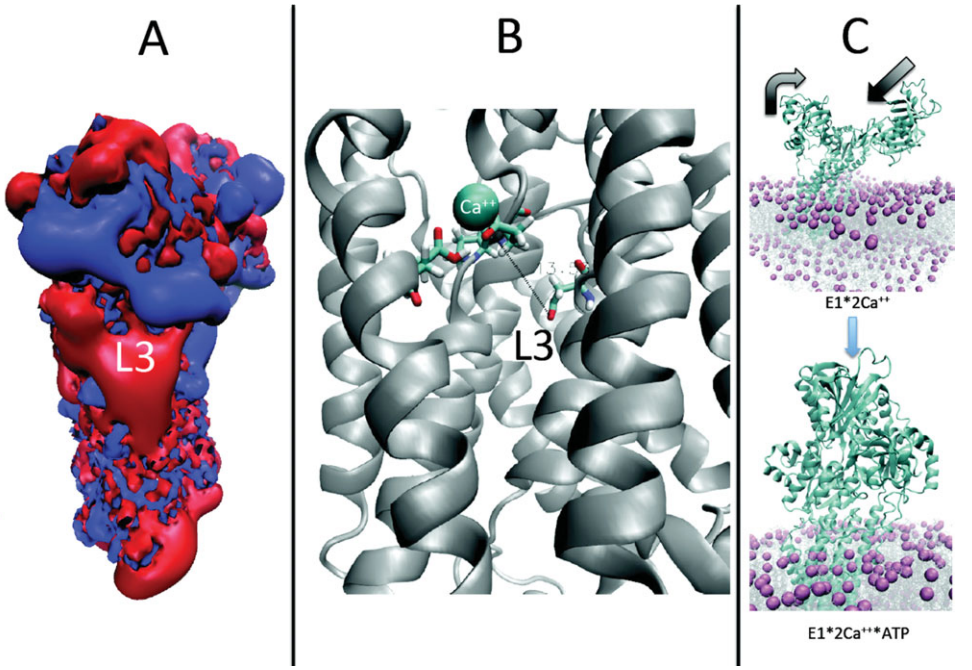

Figure 2. (a) APBS-produced electrostatic map of apo SERCA (red = −3.0 kT/e, blue= +3.0 kT/e). Brownian dynamics simulations were used to investigate cation binding to the L3 region of SERCA. (b) Umbrella sampling simulations were used to model the cation moving from the protein/solvent/lipid boundary to approximately 10 Å deep within the TM region where Ca^{2+} binding-site II is located. (c) Upon Ca^{2+} binding, a gradual motion of the N and A cytosolic domains was observed in MD simulations.

diffusion into the binding site, and allosteric signaling of the A and N domains (Fig. 2). Here, we combine Brownian dynamics to probe Ca^{2+} binding to the outer SERCA surface, umbrella sampling to explore pathways leading from the SERCA surface to site II, and molecular dynamics (MD) to examine allosteric activity associated with Ca^{2+} binding. We focus in particular on the contributions of acidic surface residues along L3, in particular the role of the gating residue E309, which together we hypothesize serve as recognition residues for guiding Ca^{2+} association.

Results

Diffusion-limited binding of Ca^{2+} to the SERCA molecular surface

We hypothesized that Ca^{2+} binding proceeds as a two step process: (1) diffusion of Ca^{2+} from the bulk to the interface between solvent and the binding channel; (2) subsequent diffusion within the binding channel to the site II binding site. To investigate the first step, we used Browndye to estimate the Ca^{2+} association rate, k_{on}, to the Ca^{2+}-free (apo) E1 state. These results are reported in Table 1. We chose reaction coordinates based on association with D813 of L1 and E309 of L3, as these residues border the postulated Ca^{2+} entryways or "vestibules." E309 is of special interest, as it both borders site II and the vestibule just outside site II along the L3 pathway. We did not observe any association events near L1, which we believe was due to the small spacing between the lipid and cytosolic domain comprising L1, as well as the presence of a positively charged residue nearby (K329). For the L3 site, however, we found significant accumulation near the L3 site that yielded a predicted Ca^{2+} association rate, k_{on}, of 3.4 ± 0.04 × 10^9 $M^{-1}s^{-1}$ at a physiological ionic strength of 0.15 M (Supporting Information, Fig. S1). To examine the role of favorable electrostatic interactions between Ca^{2+} and the negatively charged residues of the L3 vestibule, we computed k_{on} with ionic strengths ranging from 0.05–2.00 M. First, we found that k_{on} decreases with increasing ionic strength (7.9 × 10^9 down to 1.41 × 10^9) as is expected for electrostatically-driven, diffusion-limited reactions. Second, we found that k_{on} at physiological ionic strength was nearly two-orders of magnitude greater (0.06 × 10^9 $M^{-1}s^{-1}$) than at high ionic strength (200 M), where electrostatic interactions are substantially shielded, using adaptive Poisson Boltzmann Solver (APBS).

Table 1. *Predicted k_{on} Values at Various Ionic Strengths*

Ionic strength [M]	0.05	0.15	0.20	0.25	2.00	Inf
k_{on} [x 10^9 M^{-1} S^{-1}]	7.9 ± 0.08	3.40 ± 0.04	3.51 ± 0.05	3.15 ± 0.05	1.41 ± 0.3	0.062 ± 0.5

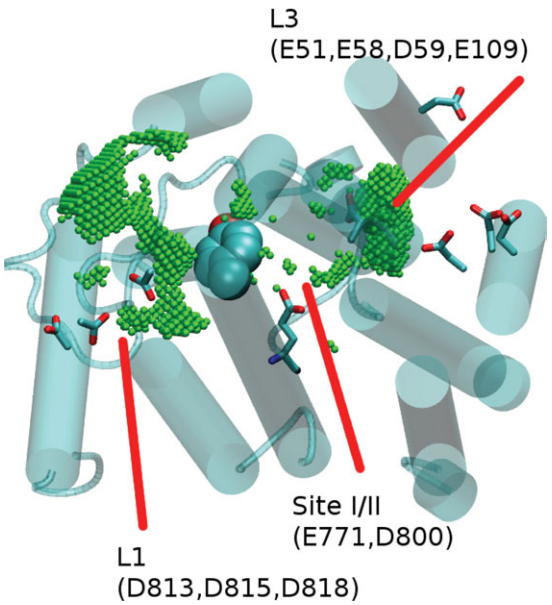

Figure 3. Top view of SERCA trans-membrane domain with L1 and L3 binding pathways and sites I and II Ca^{2+} coordination sites. Tyr 763 is represented with space-filling spheres.

Post-encounter incorporation of Ca^{2+} into the binding site

Considerable evidence suggests that Ca^{2+} binds SERCA in a cooperative manner.[18] One prominent model for sequential calcium binding implicates the rearrangement of D800, which links site I and site II, to enhance the affinity of site II for Ca^{2+} following binding at site I.[1] Here, we complement studies, in which the binding of Ca^{2+} to site I was explored, to examine the role of residues lining the L3 binding pathway in facilitating the incorporation of bulk Ca^{2+} into site II. To this end, we estimated the pathway from bulk toward D800 of the binding site using POcket Volume MEasurer (POVME) (Fig. 3), as D800 is the primary residue bridging sites I and II that coordinates both Ca^{2+} ions. POVME approximates the shape of a binding domain by placing spheres around a user-defined region and culling those that clash with the protein; as such, it can identify potential pathways bridging the protein exterior and binding domain. We considered the free space around D800 and with POVME, we identified a region that connects site II with the protein exterior corresponding to the L3 binding pathway suggested by Huang *et al*. and others.[8,13,14] Based on this analysis, it appears that the L3 vestibule is relatively open, but as one approaches E309, the solvent-accessible volume constricts to a very narrow (diameter of approximately 2 Å) and nearly linear pathway leading to site II. For the L1 case, we were unable to find a pathway that led to incorporation of the ion, as the region about Y763 bridging the L1 vestibule and site I appears to be too tightly packed, in contrast to findings from Huang *et al*.[8] One possible explanation for the discrepancy is that Huang's simulation realized an opening of this region that permitted solvent exchange between L1 and site I.

The accumulation of Ca^{2+} near the polar residues of L3 from Brownian dynamics (BD) simulations suggests the involvement of these residues in providing access to the TM binding domain. We examined conformations of the L3 residues E51, E55, D59, and E309 and found that only E309 assumes distinctly different distributions in the apo and holo states (Supporting Information, Fig. S2). In the apo form, E309 peaks at approximately 180 degrees, corresponding to a conformation pointing toward the bulk solvent. In this conformation, E309 is in nearly continuous contact with the protonated E58 (Supporting Information, Fig. S3) and provides favorable electrostatic interactions with solvated cations. In the holo form, E309 shifts to −70 degrees (toward the binding site), where it forms a known coordination interaction with Ca^{2+} in site II. In contrast, we found that other charged residues, namely E51, E55, and D59, tend to freely rotate in both the apo and holo states without any clear conformational preference and are thus unlikely to play an active role in Ca^{2+} assimilation.

To investigate the ease of diffusion into site II along the approximately 12 Å-long L3 pathway, we estimate the (PMF) along a reaction path leading from the bulk to the site II region. The trajectory, $\psi(x)$, consists of a linear path determined from POVME beginning at D800 ($\psi(x) = 2$ Å) and ending in the bulk ($\psi(x) = 26$ Å). The PMF was determined from umbrella sampling using 0.5 Å window sizes; values are reported relative to the minimum potential value at a favorable D800/Ca^{2+} coordination distance ($\psi(x) \approx 4$ Å). Far from the binding site the PMF was nearly constant at 2.0 to 2.5 kcal/mol, but decreased by almost 1.5 kcal/mol as $\psi(x)$ approached a 7 Å separation from D800. At $\psi \approx 6$ Å we note a small barrier (≈ 0.5 kcal/mol) that we attribute to the formation of a bidentate interaction between Ca^{2+} and the E309 carbonyl side chain. In this configuration, we note the loss of one water molecule in the Ca^{2+} hydration shell, as illustrated in the Supporting Information movie. As $\psi(x)$ decreased from 6 Å, E309 rapidly flipped between the binding site and solvent-exposed conformations. The binding site-facing orientation of E309 toward D800 promoted binding of Ca^{2+} via mono-dentate and bidentate interactions, respectively and thus forming the bound state, Fig. 4, which is shown in the Supporting Information movie.

Based on our findings that E309 appears to switch conformations as Ca^{2+} approaches site II, we sought to characterize its gating rate as a function of Ca^{2+} position. To this end, we identified two E309 conformational states based on our observations and the convention in[19] (1) a closed state oriented toward the binding site with a C_α/C_β angle of −70 degrees, which is typical of the holo enzyme. (2) an open

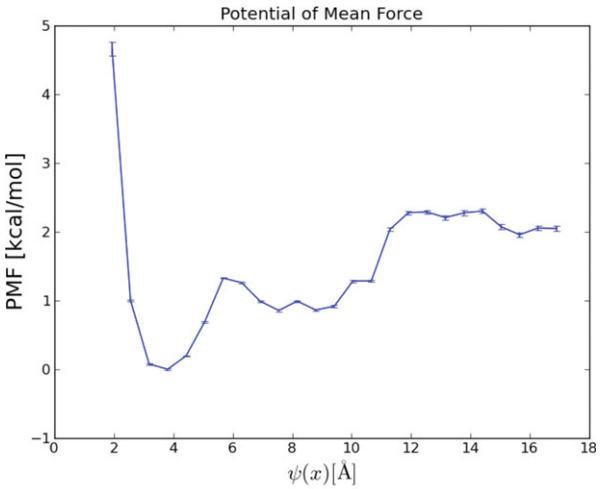

(a)

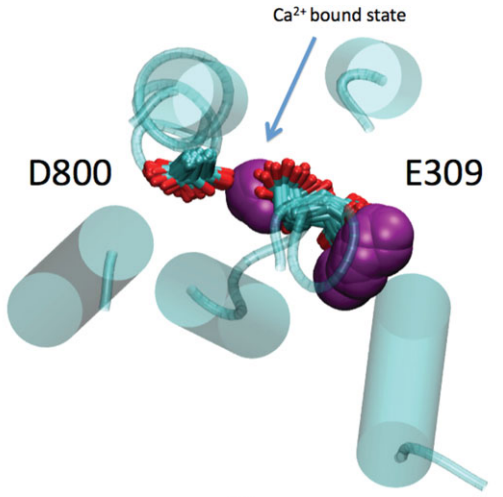

(b)

Figure 4. Potential of mean force corresponding to translation of Ca^{2+} from bulk ($\psi(x) = 18$Å) to the bound conformation with D800 ($\psi(x) = 2$Å). Figure showing gating of E309 with Ca^{2+} in purple space-filling spheres.

state, typical of the apo configuration, with a C_α/C_β angle of 180 degrees, that points the carboxylic acid toward the L3 vestibule. In Figure 5, we assign 1 (blue) when E309 assumes the open state, and 0 when closed. We find that when Ca^{2+} is far from the binding site (measured by Ca^{2+}/D800 distance in red), E309 was predominantly open (open probability, p_0, of nearly 80%), while exchanges between the open and closed states were very fast (nearly on the order of 1 ns). These data imply that there is a small energetic barrier to rotation between the two states. As Ca^{2+} approaches D800, the distribution rapidly changes and nearly entirely favors the closed state, especially after Ca^{2+} associates with E309 at t = 38 ns.

Structure and dynamics of E1 and E1(Ca)

Collective motions. To investigate the extent to which Ca^{2+} binding promotes conformational changes leading to E1P, we examined SERCA conformational motions linking the E1(Ca) and E1P states via MD. Principal component analysis (PCA) based on all available crystal structures separated 96% of structural variation into three principle modes, of which Principal Component 1 (PC1) and Principal Component 2 (PC2) captured 86% of the variance (Supporting Information, Fig. S4). The crystal structures were partitioned into four tightly clustered, well-separated states; each cluster exclusively contained structures belonging to a specific catalytic state (E1, E1P, E2, E2P). The first principal component primarily describes the transition between the E2 and E1(Ca) catalytic states (Fig. 6). The primary conformational motions involve an approximately 110 degree rotation of the cytosolic A domain in E2 structure parallel to the plane of the membrane and concurrent tilting of the cytosolic N domain away from the central TM bundle. PC1 also includes the straightening of helix M1. Helix M1 is bent along the plane of the bilayer in E2 but straightens to be nearly perpendicular to the plane of the bilayer in the E1(Ca) structure. Bundle motions were comparatively smaller, with the most obvious movement restricted to M5 progression toward M6. The second principal component (PC2) describes the transition between the E1(Ca) state and the E1P catalytic state, whereby the cytosolic domains A and N undergo a closing motion. This component corresponds to the A domain rotating perpendicular to the plane of the membrane with movement of the N domain toward the TM bundle. Together, these principal components correspond to large scale collective motions that readily partition crystallographic SERCA data into

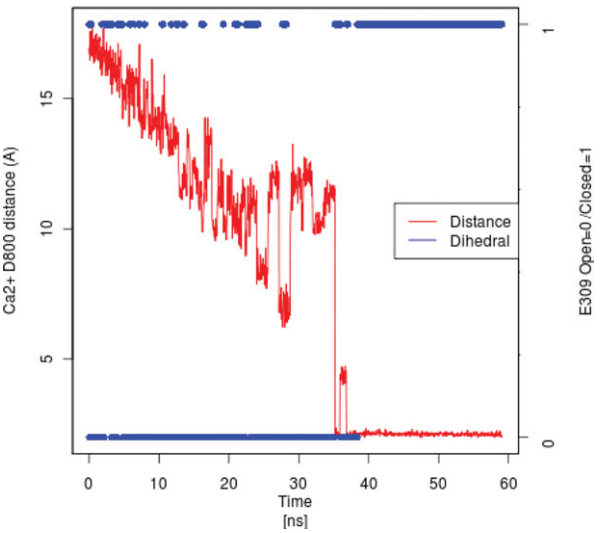

Figure 5. Plot of distance between Ca^{2+} and D800 of the bound configuration (red) versus E309 open/closed state. E309 is considered open when its C_α/C_β angle is approximately −50 degrees.

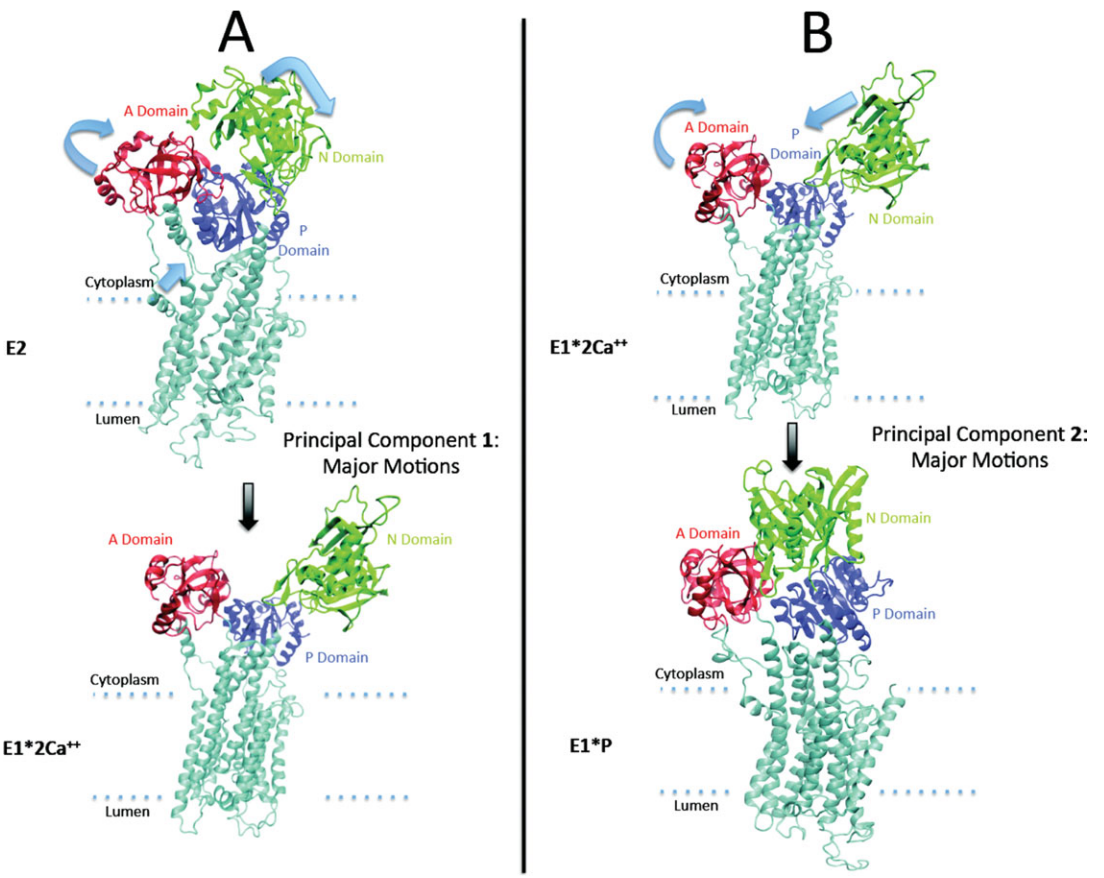

Figure 6. Left: PC1 linking E2 and E1 states. Right: PC2 linking E1 and E1P structures.

catalytically-relevant states and comprise a relevant basis for characterizing our MD simulations.

We performed four cMD simulations (run1: 2 × 75 ns and run2: 2 × 45 ns) and two aMD simulations (amd: 2 × 225 ns) of the apo and holo states to investigate dynamic consequences of Ca^{2+} binding. As the closing motion identified by PC2 is a known requirement for E1P formation upon Ca^{2+} binding, we projected our molecular dynamics simulation data along this component (and PC1) to determine the extent to which we sample the E1→E1P transition (Fig. 7). We found that for two of the three apo cases, the trajectories progressed along the negative PC2 direction away from the E1P state, and to some extent along the negative PC1 direction toward the E2 state. In contrast, the holo cases consistently approached the E1P state along PC2 and away from the E1(Ca) crystal structures.

To gain insight into the domain motions underying the E1→E1P transition, we examined the root mean squared deviations (RMSD) corresponding to the A, N, and P cytosolic domains, as well as the TM bundle from the conventional and accelerated MD simulations (Fig. 8). We consistently found that the N domain is the most mobile region of the protein with RMSDs in excess of 20 Å for some cases, while A is similarly mobile with ranges from 5–10 Å. The P domain, however, was found to be more mobile in the apo cases (run2 and amd have RMSDs around 5 Å), while all holo cases report substantially lower RMSDs (<3 Å with minor excursions). We also discovered that for the apo case in which the P domain moved comparatively little (run 1), considerable progress was made along PC2 toward E1P, in contrast to the other apo cases (run2 and aMD) (Supporting Information, Table 3).

Residue dynamics. To investigate whether these large scale conformational motions are accompanied by localized changes in the dynamics of individual domains, we examined the root mean squared fluctuations (RMSF) in the apo and holo states (Fig. 9). Independent of Ca^{2+}, we report large RMSF values indicating that the cytosolic domains A (red), N (green), and P (blue), as well as the cytosol-exposed TM bundle loops (L12, L34, L67 and L89) were relatively mobile compared to the rigid TM bundle (purple). Among the TM loops, the L67, and L89 (black) bordering the hypothesized L1 binding pathway, were comparatively more rigid than the L12/L34 loops along the L3 binding pathway. These findings are in agreement with Costa *et al.*[14], although in contrast, Huang *et al.*[8] found that L67 was quite

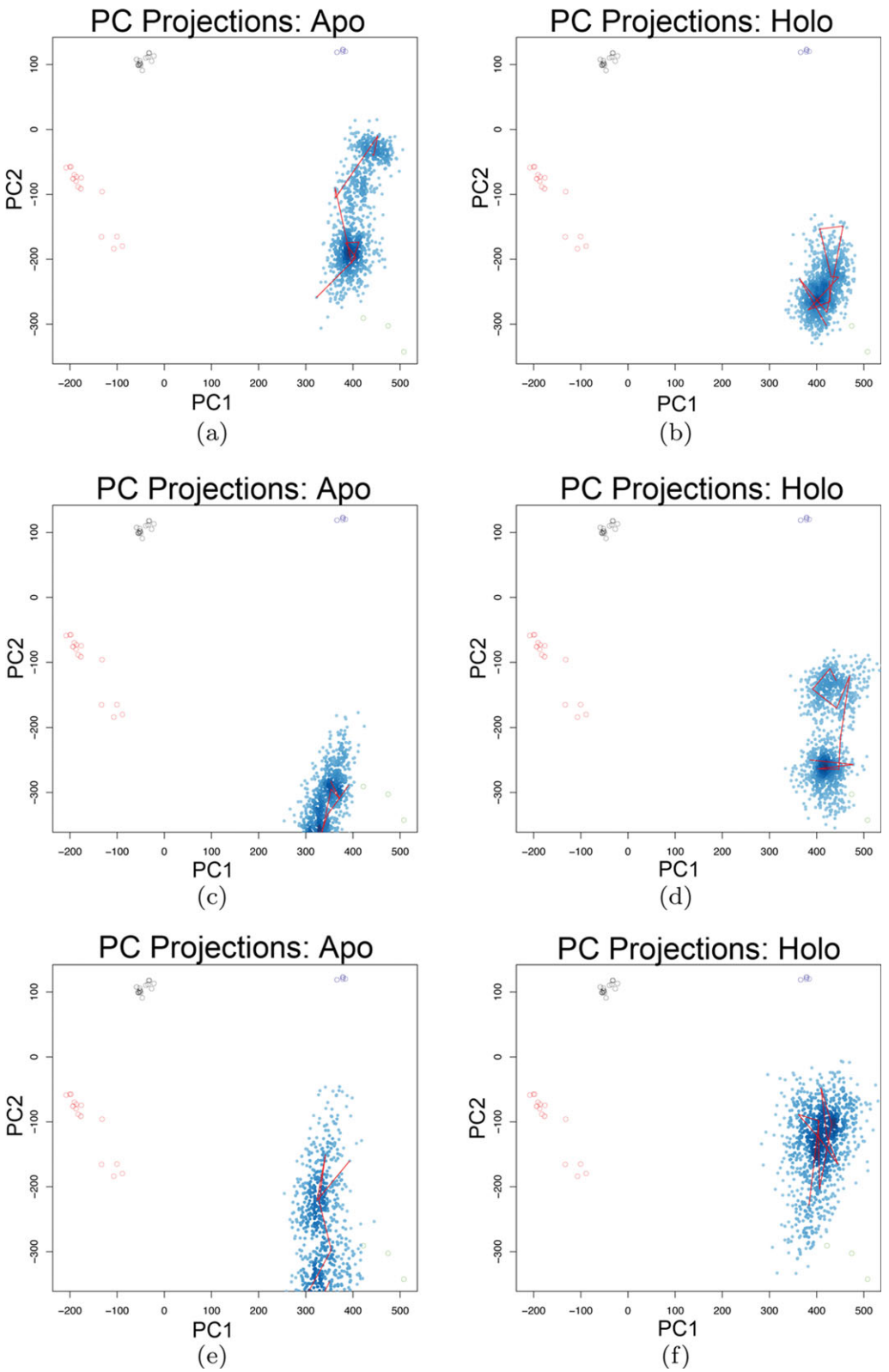

Figure 7. PCA projections of 75 ns conventional MD run 1 (top), 45 ns conventional MD (middle), and 225 ns aMD (bottom) simulations of (a,c) apo and (b,d) holo states. PC2 (y axis) and PC1(x axis) separate crystallographic data into distinct regions: E1(green), E1P (blue), E2P (black) and E2 (red).

mobile; the discrepancy is very likely due to the difference in simulation lengths and sensitivity to initial conditions. Upon binding Ca^{2+}, we observe consistent increases in RMSF for A domain (red, +15–35% change in RMSF over amino acids in domain) and bundle loop L34 (+10–50%) across all holo simulations (Supporting Information, Fig. S5). While large changes were also noted for the N domain (green, >10%) and

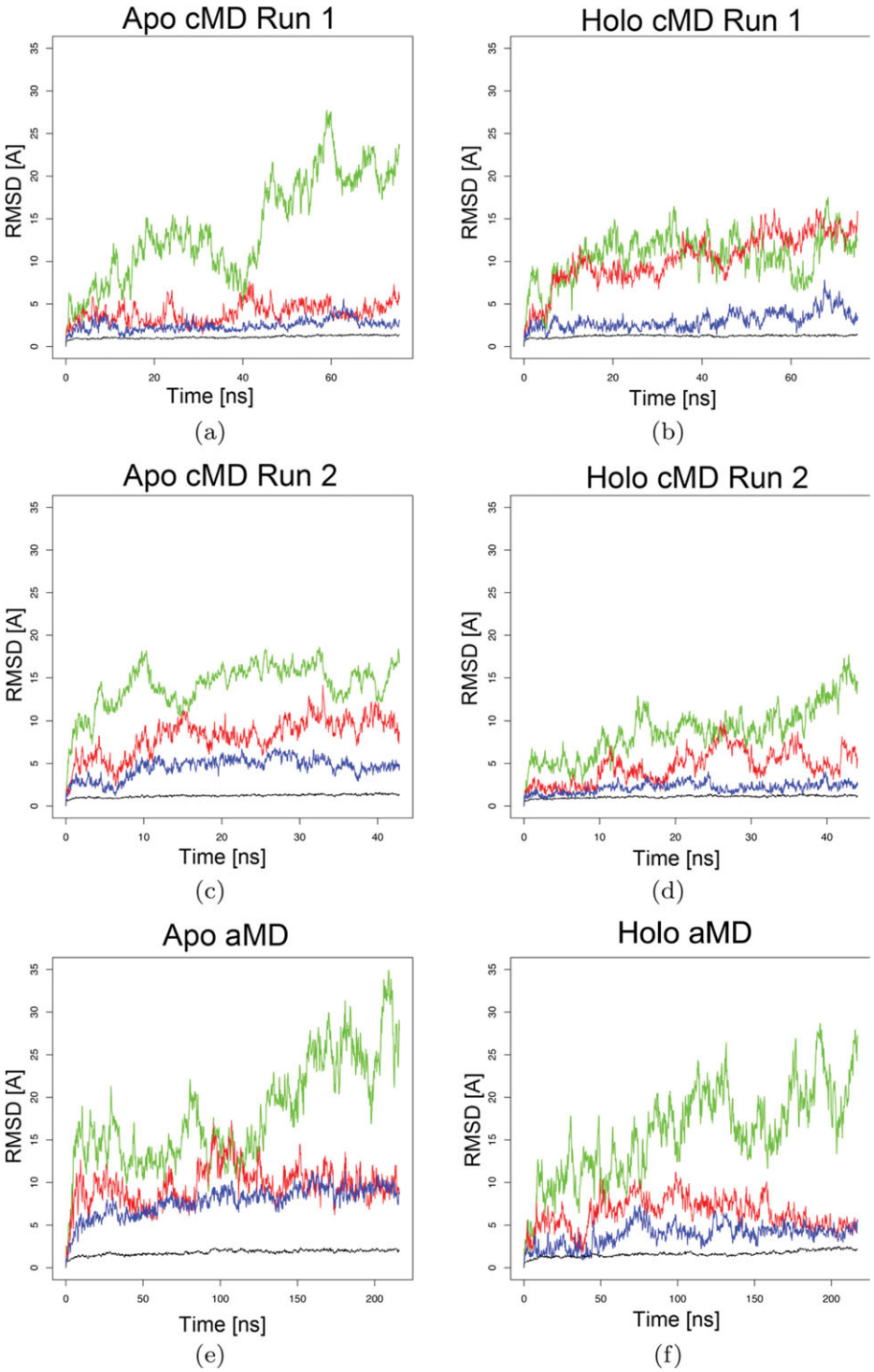

Figure 8. Overall RMSD for domains A,N, and P (a,c,e) apo and (b,d,f) holo configurations. Rows correspond to cMD run 1 (a,b), cMD run 2 (c,d) and aMD run (e,f). Plots are colored according to cytosolic domains A (red), N (green), P (blue), and bundle helices (purple).

the loops linking the bundle and cytosolic domains (gray, >5–15%), both increases and decreases were observed without any clear correspondence to the apo versus holo states. Thus, while little change in fluctuations was noted within the bundle where Ca^{2+} binds, it is apparent that binding allosterically impacts the dynamics of distant regions of the protein.

Discussion

Diffusion-limited Ca^{2+} binding

Brownian dynamics studies reveal that Ca^{2+} binding is diffusion-limited, guided by electrostatic interactions and impacted by E309 gating. Ref. 17, 18 reported apparent equilibrium constants ranging from 0.32 to 2.3 μM for several SERCA isoforms;

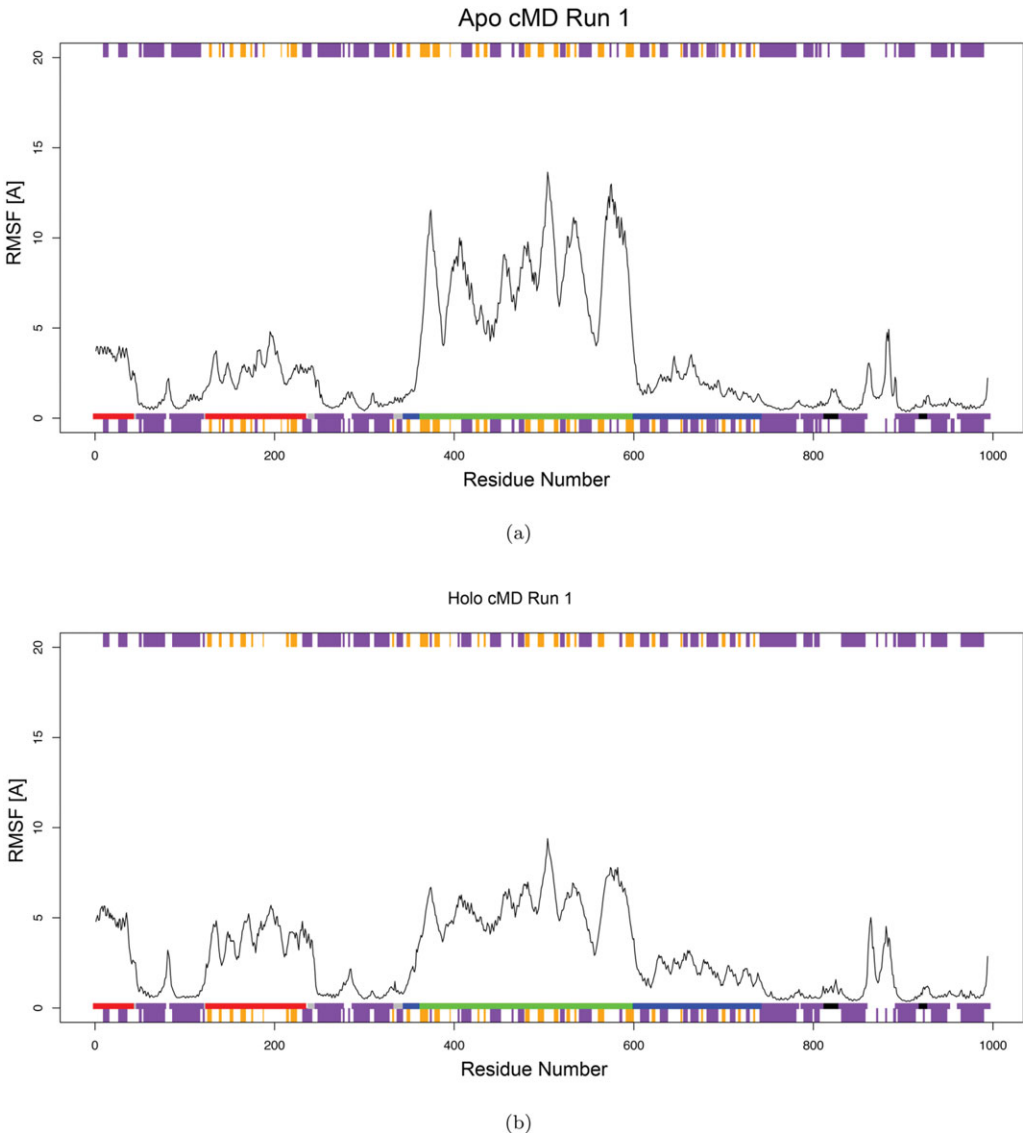

Figure 9. RMSF distribution for (a) apo and (b) holo based on cMD run1 1 simulation. Residues are colored according to cytosolic domains A (red), N (green), P (blue), cytosolic loops (gray/yellow), bundle helices (purple), and bundle loops (black).

assuming k_{off} is roughly 0.1 s^{-1},[20] these equilibrium constants suggest k_{on} could range from 1.2×10^6 and 5×10^8 $M^{-1}s^{-1}$. While our predictions of 3.13×10^9 $M^{-1}s^{-1}$ are within the diffusion-limited regime, they are between one and three orders of magnitude faster than experimental estimates. Nevertheless, the very fast association rate suggests the importance of strong electrostatic interactions between SERCA and Ca^{2+}, which is a common mechanism for achieving large diffusion-limited rates in a variety of enzyme reactions.[21]

The contribution of favorable electrostatic interactions is evidenced by the accumulation of BD Ca^{2+} trajectories near the negatively-charged region at L3 (particularly at E51, E55, E58, D59, E109 in agreement with.[10,13]) Furthermore, we showed that k_{on} at physiologically-relevant ionic strength is nearly two-orders of magnitude faster than when a purely hypothetical ionic strength is used to nullify the electrostatic interactions. We considered the possibility that the electrostatic driving force might vary due to the highly mobile charged amino acids or the occasional lipid headgroup diffusing toward the binding pathway, and these variations may partially explain the discrepancy between our predictions and experimental estimates of k_{on}. However, we obtained very similar Brownian dynamics association rates using a multitude of SERCA structures, which suggests that the long-ranged electrostatic driving force is relatively insensitive to the SERCA conformational state or lipid configuration.

Therefore, we believe the disparity between our predicted and experimentally observed k_{on} estimates may in fact be due to post-encounter effects occurring after the initial association of Ca^{2+} with the SERCA exterior. One potential post-encounter effect, gated access to site II via E309 suggested by experimental[10] and computational studies,[16] may partially account for the difference between theoretical and

experimental estimates of k_{on}. According to Ref. 22, the impact of a gated binding site on the observed association rate, $k_{on,obs}$, can be estimated by comparison of the gating rate, ω, to the characteristic diffusion time of the substrate, τ_d, to escape the binding site. If $\omega \gg \tau_{d^{-1}}$, a fast limit is obtained in which $k_{on,obs} = k_{on}$; for $\omega \ll \tau_{d^{-1}}$ a slow limit is obtained, in which the association rate is weighted by the probability of that the gate assumes the holo configuration, p_h ($k_{on,obs} = p_h\ k_{on}$). Assuming for simplicity a diffusion constant of $D = 7.7$ cm^2/s for a bare Ca^{2+} ion and an escape distance one Debye length $x \approx 7$ Å ($1\times\ 10^{-7}$ cm), we might anticipate $\tau_d \approx 10$ ns using $x^2 = 6D\tau_d$, which places our system within an order of magnitude of the slow-gating regime. Combining the estimated holo probability ($p_h = 1 - p_o \approx 20\%$) and the slight PMF barrier (0.5 kcal/mol) could reduce our k_{on} by an order of magnitude and within experimental estimates. Numerical estimation of the local diffusion constant would be necessary to more adequately describe the binding kinetics, and is the subject of further inquiry. Additional considerations, such as including polarization effects due to Ca^{2+}, and assessment of the entropic change during the dehydration of Ca^{2+}, could also significantly impact k_{on}.

Binding pathways

M6/M7 (L1)[12,23] and M1 (L3)[10] have been proposed as potential pathways in early MD studies.[8,14] However, recently Musgaard *et al.*[13] provide convincing electrostatic and molecular dynamics evidence that only L3 supports binding. Our studies confirm their findings, and also demonstrate that ligand-dependent E309 gating is further involved in Ca^{2+} entry. Based on BD results, the accumulation of Ca^{2+} near L3 and not L1 suggests the possibility that only the former supports cation association, in agreement with findings from Musgaard *et al.*[13] To further rule out the possibility of Ca^{2+} entry via L1, we examined solvent exchange into L3 and L1 from our MD studies as a probe for Ca^{2+} entry and found the water exchanges more freely at L3 than L1 (data not shown). We attribute this to two factors: (1) there is a significant deformation of the lipid bilayer near L3 found in this study and others[24,25] that provides a larger interfacial area for solvent entry and (2) the relatively rigid L67/L89 regions evidenced by RMSF constitutes a restrictive gateway to solvent exchange. These findings, together with our POVME calculations showing no clear pathway between L1 and site I, challenge the idea of L1 serving as a Ca^{2+} binding route in absence of substantial rearrangement. Nevertheless, it is possible that ions with smaller effective radii or coordination shells could diffuse into or out of L67/L89, such as the proton release from E309/E771 preceding the E1→E1P transition.[13]

For Ca^{2+} binding at L3, the ion must diffuse from the solvent-exposed vestibule toward the buried Ca^{2+} binding site. Our estimates of the PMF along this pathway (from just prior to association with E309) suggest favorable electrostatic interactions between Ca^{2+} and the negatively-charged residues lining the L3 region facilitate Ca^{2+} entry. Impeding binding, however, is a barrier between the L3 vestibule and site II where E309/Ca^{2+} interactions predominate. The barrier characterized in this study involves both a rotation of the E309 χ_1 angle and a reduction in the water coordination number of Ca^{2+}. In our simulations, the energetic cost of dehydrating Ca^{2+} in order to traverse the narrow binding region underneath E309 appears to be offset by the bidentate coordination of Ca^{2+} with the carboxylic acid. These findings could explain why E309Q[19] and E309D[20] increase Ca^{2+} dissociation, as E309Q could disrupt Ca^{2+} coordination and E309D could widen the pore leading out of site II. Thus, these factors together could constitute a filter selective for Ca^{2+} relative to K^+ and Mg^{2+}. Investigating the interplay between E309 gating rates and PMFs associated with K^+, Ca^{2+}, and Mg^{2+} entry may provide further insight into this phenomenon.

Site I residues serve an important role for stabilizing Ca^{2+} within site II, particularly when already occupied by the first bound Ca^{2+}. In particular, site I bound Ca^{2+} orients the D800 backbone carbonyl oxygen toward the site II binding site, thereby presenting a necessary coordination oxygen for site II Ca^{2+} binding. While we expect the potential of mean force near $\psi = 0$ Å to vary depending on whether site I is occupied by Ca^{2+}, we do not expect the electrostatic component to the PMF to change considerably beyond $\psi = 2$ Å, therefore, our estimates of the E309 gating rate and diffusional encounter of Ca^{2+} should be comparable. We base this speculation on the abundance and relative mobility of charged amino acids in site I, which would likely screen the strong positive charge of a bound Ca^{2+}. We believe this speculation is in line with findings from Musgaard et al,[18] who showed that cation accumulation in the binding region is found in both their apo and bound states, therefore, evidencing a similar electrostatic field near the binding region. Nevertheless, local variations, such as differences in the relative order of M4 between the E2 and E1(Ca) states,[14] could impose additional steric barriers to Ca^{2+} diffusion.

Protein dynamics

It is apparent from crystallographic data that Ca^{2+} binding to the apo E1 state induces conformational changes that promote formation of the ATP-bound E1P state. Our data underestimate this conformational change, yet nevertheless demonstrate that binding of Ca^{2+} alters loop and cytosolic domain

dynamics. While we found that the motions of the cytosolic domains varied considerably between simulations, we found trends that could explain the effects of Ca^{2+} binding. One particularly interesting trend is the correlation between motion of the P domain and progression toward E2, whereas motion along PC2 toward E1P seems to occur spontaneously when the P-domain is immobile. As the P domain is consistently immobile in the Ca^{2+} state, and mobile for two of the three apo simulations, it is possible that Ca^{2+} binding shifts the equilibrium between P-mobile and P-fixed states and thus increases the likelihood of progressing toward the E1P state relative to the apo. Interestingly, we also observed that the most probable conformation indicated by principal component (PC) space was somewhat distinct from the crystal structures suggesting that the stable A/N distance is smaller than the crystal structure, as concluded from fluorescence resonance energy transfer (FRET) experiments.[2] Hence, the structural data obtained from x-ray crystallography may benefit from inquiry into the dynamics underlying SERCA function that is afforded by MD simulation and dynamical measurements such as FRET and nuclear magnetic resonance (NMR).

This MD study and that of Espinoza-Fonseca *et al.*[17] also consistently found that Ca^{2+} binding alters the dynamics of the cytosolic domains in the absence of major bundle rearrangement. As such, it is possible that they contribute an entropic driving force toward conversion to the E1P state upon ATP hydrolysis, which would help explain its temperature-dependence.[9] An additional contribution of enhanced motion of the cytosolic domains toward E1P via immobilization of the P domain is the promotion of ATP binding by decreasing the distance between doamin A and D351 of domain P, thus enabling the latter's phosphorylation.[17] Upon ATP binding, sufficient free energy would be provided to promote substantial bundle rearrangement that ultimately stabilizes the E1P structure. This stepwise-interpretation would explain why there is an estimated millisecond timescale for the E1→E1P transition observed experimentally,[26] despite possible submicro-second A/N closing dynamics observed in MD studies.[17]

As a whole, we did not observe significant rearrangements of bundle helices upon Ca^{2+} binding. We anticipated that in absence of Ca^{2+}, the disordered region of M4 near E309 reported in the E1 state would reform the alpha helix found in E2 upon binding as was assumed in the MD study from.[14] We instead found that M4 remained disordered, which we propose facilitates the transfer of Ca^{2+} from the binding vestibule into site II via E309. It is possible that protonation of E309 and E771, as expected in the E2 state,[9] may be required to reestablish the helical region in the disordered region about E309.

Despite little change in the structure of M4, we found the magnitude of fluctuations (RMSF) for the L34 loop was increased in the holo state. Based on the enhanced cytosolic domain and loop mobility in absence of bundle rearrangement, we postulate that one effect of Ca^{2+} binding is that the TM bundle is locked in place, thereby promoting a redistribution of vibrational motion to the cytosolic domains. Shifting of fluctuations upon substrate binding has been observed in other systems by NMR[27] and simulation,[28] and may constitute a common mechanism of allosteric signaling. As M4 has been postulated as a transducer of the signal between the Ca^{2+} binding site and phosphorylation regions of the P-domain,[1,29] it is possible that enhanced fluctuations of L34 may allosterically contribute to dynamics along PC1 and PC2 by modulating P domain mobility. In contrast, L67 and L89 were found to be quite rigid, which may help lock the TM bundle with the P domain and thereby promote progression toward E1P. Disrupting this lock might then be expected to reduce ATPase turnover, as was observed by[12] for L67 at the D813, D815, and D818 positions. Overall, however, changes in SERCA conformational dynamics due to Ca^{2+} are anticipated to be small relative to those induced by ATP binding.[30]

Limitations

In this study, we chose an apo state based on removal of Ca^{2+} from the E1(Ca) structure, in line with Refs. 17,25. Experimental data suggest that at least one additional choice of apo state may be possible.[12,31] In Refs. 31, Trp quenching was measured during sequential binding of Ca^{2+}, which suggested a conformational difference between the E1(Ca) and E1 free states. Specifically, the data suggest that binding of Ca^{2+} to site I does not change the fluorescence signal, whereas site II binding leads to a drop indicative of a conformational change that might not be apparent in our model choice. However, we believe it is reasonable to anticipate that fluorescence does not give a strong indication of the amplitude of such conformational changes.[2] Furthermore, it is not clear from the experiment, which TM Trp were impacted by the conformational change, and whether these changes are evidence of differences in the L3 binding vestibule considered in our study. Given that the nearest Trp to site II is 12 angstroms from the L3 vestibule, and the other eleven Trp are toward the periphery of the bundle, it is equally possible that quenching indicates distant conformational changes not pertinent to the Ca^{2+} binding domains. In our opinion, there is not sufficient evidence to rule out our choice of model.

One possibility to reconcile the apparent contradiction between our model and the Lenoir experiment is that several apo states are in

thermodynamic equilibrium, and the population of these states is dependent on pH and Mg^{2+}, which are important factors in SERCA turnover. Binding of Ca^{2+} then, may shift this population to favor the E1(Ca) state, similar to what had been endorsed by Winters *et al.* (2008) for the cytosolic SERCA domains. Thus, our starting point with the E1(Ca) state could represent one of the possible states for Ca^{2+} binding.

In fact, we believe that our model may be the most representative conformational under physiological conditions, based on findings from Inesi *et al.*[9] In this study, it is suggested that deprotonation of E309 and E776 favors conversion to the E1 state, even in absence of Ca^{2+} binding, in contrast to the findings of Lenoir *et al*. One difference between the preparations is that the Lenoir experiment was conducted in Mg^{2+} free conditions, whereas Inesi appeared to use 3 mM Mg^{2+}, which is a more representative concentration in physiological systems. Therefore, the findings of Ref. 31 might not be universal and thus it is our opinion that a change in SERCA protonation state, as done by us and argued by others,[17] should be adequate to represent the apo structure.

It is further possible that the apo state might bear closer resemblance to the E2 structure as opposed to the E1(Ca). We note that in Ref. 13, the E2 (3NAL) structure was used as a starting point for apo simulations to explore cation binding pathways toward (but not into) sites I and II. Here, the authors state that the E2 structure corresponds to the conformation just prior to Ca^{2+} binding in which the binding sites are occluded. Comparison of the E2 and E1(Ca) structures suggest that the M4 helix unwinds near the Ca^{2+} binding domain and M1 straightens. As the E2 structure does not bind cytosolic calcium (see Fig. 4 in[13]), whereas the E1(Ca) does, we believe it is plausible that M4 and M1 require rearrangement before Ca^{2+} may be bound. Indeed our PC analysis indicates that the majority of conformational motion linking the E2 and E1(Ca) state owes to the cytosolic domains and these helices, though preliminary simulations with the E2 structure did not indicate significant motion of these components. As we do not anticipate that the E1 apo state would be drastically different from all other known SERCA crystallographic structures, we believe it is likely that the conformational changes due to sequential binding of Ca^{2+} to prevent open exchange of site I Ca^{2+} with solvent may be subtle and are thus not likely to influence our modeling of Ca^{2+} association and protein dynamics to a large degree.

Summary and conclusions

Our study explores Ca^{2+} binding as a three stage binding model consisting of (1) rapid binding of ion to the SERCA exterior, (2) fast entrance of the ion into the binding site via L3 and 3) slow time-scale reorganization of binding site that initializes allosteric signaling to the cytosolic domains (Fig. 2). Diffusion-limited, electrostatically-driven binding of Ca^{2+} to the SERCA surface is supported by kinetic measurements[29,26] and our simulated k_{on} experiments. The role of negatively charged amino acids in L3 and especially E309 in escorting surface-bound Ca^{2+} to the binding site is supported by mutagenesis studies,[19] as well as our PMF simulations. The development of an allosteric signal between the TM region and the cytosolic domains upon Ca^{2+} binding is supported by FRET studies[2,32] of M4 and M6, as well as our MD data and in particular, differences in RMSF between apo and holo states.

We believe these analyses complement those of Espinoza *et al.* and provide additional insight into the basis of conformational motion due to the presence of Ca^{2+} in the calcium binding sites. Namely, we found that that free movement of the P domain tends to lead to propagation toward the E2 state, whereas reduced movement of P domain leads to the ATP bound state. Binding of Ca^{2+} was consistently found to reduce P-domain movement. Moreover, by performing several calculations, we show that dynamics of the receptor change significantly, and suggest that a single trajectory may be one of many possible pathways.

This model may constitute a general allosteric mechanism governing the P-type ATPase family, of which SERCA is a representative member. Furthermore, our model opens doors for strategies for controlling SERCA activity including mutation of uncharged surface residues to acidic residues to further increase k_{on} and modification of bundle and cytosolic residues to modulate allosteric signaling.

Methods

Molecular dynamics

The Ca^{2+}-bound (holo E1(Ca) SERCA state, PDB id 1SU4) was obtained from the RCSB Protein Databank; the Ca^{2+}-free state (holo) was obtained by removal of the two coordinated Ca^{2+} ions. ProPka[33] was used to assign protonation states to the ionizable residues. Following Ref. 16, E58 and E908 were protonated for the holo state; E771 and D800 were protonated in the apo state in accordance with Ref. 34. Based on Ref. 9, and 35, E309 is deprotonated to simulate the E1(Ca) state. Thus, we elected to remove the Ca^{2+} ions from the holo enzyme and allow sufficient reorganization of the protein using molecular dynamics. Indeed, our simulations reveal conformational changes near the calcium binding domains upon removal of Ca^{2+}, predominantly involving E309. The soundness of this approach was demonstrated in,[17] in which the Ca^{2+}-dependent,

catalytically-relevant motions of the SERCA cytosolic domains were examined in the presence and absence of Ca^{2+}.

The psfgen package in visual molecular dynamics (VMD)[36] was used to apply patches for ionizable residues and also for disulfide bonds between C636-C675 and C876-C888. The structure was inserted into a 1-palmitoyl-2-oleoylphosphatidylcholine (POPC) lipid bilayer of dimension 140 × 140 angstroms with 483 POPC molecules using the VMD 1.9 Membrane Builder Tool. TIP3P solvent molecules were added to the space above and below the POPC lipid bilayer around the protein. 0.15M equivalents of K+ and Cl- were added to neutralize the system and resemble typical intracellular concentrations of the electrolyte. The CHARMM27 force field with NBFIX[37] was used for parameterization of all atoms. The system was partially equilibrated using NAMD 2.8b3[38] with all atoms fixed except for the lipid tails that were allowed to melt at 310 K. Next, 1000 2 fs steps of additional equlibration were performed with only the protein fixed. The system was then equilibrated with no fixed atoms at constant pressure for 0.5 ns prior to production conventional (cMD) and accelerated (aMD) MD runs. Production cMD and aMD simulations were performed with an NVT ensemble using a 2 fs timestep and periodic boundary conditions; 12.0 Å cutoffs were used for non-bonded terms, and tolerance, interpolation order and grid spacing were set to 1×10^{-6}, 4, and 1.0 Å, respectively, for the Particle-Mesh Ewald algorithm.[39] aMD simulations utilized the dihedral-boost method[40] implemented in NAMD 2.8b3, with a threshold dihedral energy value of 35,100 kcal/mol and acceleration factor $\alpha = 1{,}820$ kcal/mol. All other preparations follow from the conventional MD simulations. For this study we refer to three sets of simulations: cMD run1 (2 × 75 ns for apo and holo configurations), cMD run 2 (2 × 45 ns) and aMD (2 × 225 ns).

Principal component analysis

Principal component analysis of all homologous SERCA pump structures (approximately 40 structures with ≥ 70% sequence identity) was performed using Bio3D.[41] Bio3D identified an invariant core, which refers to the set of atoms with the smallest variation across available crystal structures. This invariant core was predominantly comprised of P-domain residues (620–624, 636–642, 653, 654, 657–667, 669–671, 674–678, 683, 686–692, 696–699) and a small loop region spanning M4 and the N domain (347–352). All structures were aligned to the invariant core for subsequent PCA. For convenience, we have summarized the key SERCA domains and their constituent amino acids in Supporting Information Table 2.

POVME

POVME v1.1.0[42] was used to determine the solvent accessible volume around the L1 and L3 vestibules. The pocket-encompassing region was computed using an initial set of spheres at 0.5 Å intervals within 30 Å of E309 of L3 and D813. Spheres in this region that intersected with the protein were culled by using a padding radius of 1.4 Å. Using VMD, we displayed the remaining spheres with VDW radii of 1.4 Å and identified connected sets of spheres bridging the protein exterior and E309/D813.

Browndye

Browndye[43] was used for Brownian dynamics simulations of Ca^{2+} binding to SERCA structures generated from MD. We selected ten structures to determine if the k_{on} rates were dependent on conformation. We included explicit lipids in these simulations from the MD-equilibrated structures, as they prevented spurious diffusion of Ca^{2+} into the TM bundle where the lipid-bilayer would typically be found. PDB2PQR[44] using the CHARMM27[37] force field for atomic charges and radii was used to generate APBS input. APBS v1.2.1[45] was used to compute the electrostatic potential using the linearized Poisson-Boltzmann equation assuming an ionic strength of 150 mM. 500,000 simulation trajectories were used to determine k_{on} association rates according to the NAM algorithm.[46] Browndye assumes a spherical reaction geometry for which k_{on} scales as $4\ \pi\ D\ R$, where D is the diffusion constant and R is the radius of the reacting sphere. For a planar geometry with a reacting disk of radius R, k_{on} scales as $4\ D\ R$.[22] Therefore, we anticipate a factor of π error in the predicted k_{on} s.

Umbrella sampling

A truncated version of the SERCA site II was created by selecting all contiguous residues within 10 Å of E309, including residues 47–60 (M1), 98–112 (M2), 300–315 (M4), 758–771 (M5), and 790–807 (M6). Our choice of truncation was based on the observation that these helices changed insignificantly over the course of our simulations. Hence, a truncated system for which the helices are constrained to their average position constitutes a suitable model for potential of mean force calculations, similar to the protocol described in Ref. 47. While bilayer lipids border the exterior of the L3 vestibule, they do not appear to enter the L3 vestibule where the PMF calculations are performed; rather, their contribution is included in the Browndye calculations. We defined our reaction coordinate in 0.5 Å intervals along L3 based on the connected set of spheres yielded by POVME; this linear trajectory led from the bound configuration (single ion) to an arbitrary region in the solvent (22 Å separation). For the bound configuration, we chose coordination with D800 in site II,

since experimental studies[7] indicate that site I binding precedes site II, and D800 is the primary residue that bridges the site I and site II. For each window, the ion was constrained to the appropriate position using a force constant of 10.0 kcal/mol, and then equilibrated for 2 ns. Statistics were collected for 6.0 ns per window following equilibration. PMF determination followed from application of the WHAM protocol (26 bins, 310K), including 50 Monte Carlo trials for bootstrap analysis of statistical error.

Trajectory analysis

The Bio3D[41] package was used to analyze MD trajectories. MD trajectories were projected along the first and second PCs identified from the available crystal structures and hierarchically clustered according to the Mahalanobis distance in PC space. The top ten structures were selected for estimation of diffusion-limited Ca^{2+} binding rate.

Acknowledgment

The authors thank Jeff Wereszczynski, Yi Wang, and Peter Tieleman for interesting discussions and careful reading of the manuscript. The computations were in part performed on Kraken at the National Institute for Computational Sciences (http://www.nics.tennessee.edu/) and the DAVinCI cluster acquired with funds from NSF. This work used the Extreme Science and Engineering Discovery Environment (XSEDE), which is supported by NSF.

References

1. Toyoshima C. (2008) Structural aspects of ion pumping by Ca2+-ATPase of sarcoplasmic reticulum. Arch Biochem Biophys 476:3–11 .
2. Winters D, Autry J, Svensson B, Thomas D. (2008) Interdomain fluorescence resonance energy transfer in SERCA probed by cyan-fluorescent protein fused to the actuator domain. Biochemistry 47:4246–4256.
3. Lewis S, Thomas D. (1992) Resolved conformational states of spin-labeled calcium-ATPase during the enzymic cycle. Biochemistry 31:7381–7389.
4. Toyoshima CC, Asahi MM, Sugita YY, Khanna RR, Tsuda TT, MacLennan DHD. (2003) Modeling of the inhibitory interaction of phospholamban with the Ca2+ ATPase. Proc Nat Acad Sci 100:467–472.
5. Toyoshima C, Inesi G. (2004) Structural basis of ion pumping by CA(2+)-ATpase of the sarcoplasmic reticulum. Annu Rev Biochem 73:269–292.
6. Rensen, TL-MlS, Ller JVM, Nissen P. (2004) Phosphoryl transfer and calcium ion occlusion in the calcium pump. Science. 304:1672–1675.
7. Zhang Z, Lewis D, Strock C, Inesi G, Nakasako M, Nomura H, Toyoshima C. (2000) Detailed characterization of the cooperative mechanism of Ca 2+binding and catalytic activation in the Ca 2+transport (SERCA) ATPase. Biochemistry 39:8758–8767.
8. Huang Y, Li H, Bu Y. (2009) Molecular dynamics simulation exploration of cooperative migration mechanism of calcium ions in sarcoplasmic reticulum Ca 2+-ATPase. J Comput Chem 30:2136–2145.
9. Inesi G, Lewis D, Toyoshima C, Hirata A, de Meis L. (2008) Conformational fluctuations of the Ca2+-ATPase in the native membrane environment. J Biol Chem 283:1189.
10. Lee A, East J. (2001) What the structure of a calcium pump tells us about its mechanism. Biochem J 356: 665.
11. Einholm AP. (2004) Importance of transmembrane segment M1 of the sarcoplasmic reticulum Ca2+-ATPase in Ca2+ occlusion and phospho-enzyme processing. J Biol Chem 279:15888–15896.
12. Zhang Z, Toyoshima C. (2001) The role of the M6–M7 Loop (L67) in stabilization of the phosphorylation and Ca2+ binding domains of the sarcoplasmic reticulum Ca2+-ATPase (SERCA). J Biol Chem 276:15232–15239.
13. Musgaard M, Thogersen L, Schiott B, Tajkhorshid E. (2012) Tracing cytoplasmic Ca2+ ion and water access points in the Ca2+-ATPase. Biophys J 102:268–277.
14. Costa V, Carloni P. (2003) Calcium, binding to the transmembrane domain of the sarcoplasmic reticulum Ca2+-ATPase: insights from molecular modeling. Prot-Struct Funct Bioinformatics 50:104–113.
15. Sugita Y, Ikeguchi M, Toyoshima C. (2010) Relationship between Ca2+-affinity and shielding of bulk water in the Ca2+-pump from molecular dynamics simulations. Proc Nat Acad Sci 107:21465–21469.
16. Sugita Y, Miyashita N, Ikeguchi M, Kidera A, Toyoshima C. (2005) Protonation of the acidic residues in the transmembrane cation-binding sites of the Ca2+ pump. J Am Chem Soc 127:6150–6151.
17. Espinoza-Fonseca LM, Thomas DD. (2011) Atomic-level characterization of the activation mechanism of SERCA by calcium. PLoS ONE. 6:e26936.
18. Inesi G, Kurzmack M, Coan C, Lewis DE. (1980) Cooperative calcium binding and ATPase activation in sarcoplasmic reticulum vesicles. J Biol Chem 255: 3025–3031.
19. Inesi G, Ma H, Lewis D, Xu C. (2004) Ca2+ occlusion and gating function of Glu309 in the ADP-fluoroaluminate analog of the Ca2+- ATPase phosphoenzyme intermediate. J Biol Chem 279:31629.
20. Sorensen TLT, Dupont YY, Vilsen BB, Andersen JPJ. (2000) Fast kinetic analysis of conformational changes in mutants of the Ca(2+)- ATPase of sarcoplasmic reticulum. J Biol Chem 275:5400–5408.
21. Wade RC, Gabdoulline RR, LÃdemann SK, Lounnas V. (1998) Electrostatic steering and ionic tethering in enzyme-ligand binding: insights from simulations. Proc Nat Acad Sci 95:5942–5949.
22. Szabo A, Shoup D, Northrup S, McCammon J. (1982) Stochastically gated diffusion-influenced reactions. J Chem Phys 77:4484–4493.
23. Toyoshima C, Nakasako M, Nomura H, Ogawa H. (2000) Crystal structure of the calcium pump of sarcoplasmic reticulum at 2.6 —[angst]— resolution. Nature 405:647–655.
24. Sonntag Y, Musgaard M, Olesen C, Schiott B, Moller JV, Nissen P, Thogersen L. (2011) Mutual adaptation of a membrane protein and its lipid bilayer during conformational changes. Nat Commun 2:304.
25. Lervik A, Bresme F, Kjelstrup S. (2012) Molecular dynamics simulations of the Ca2+-pump: a structural analysis. Phys Chem Chem Phy 14:3543.
26. Dode L, Vilsen B, Van Baelen K, Wuytack F, Clausen J, Andersen J. (2002) Dissection of the functional differences between sarco (endo) plasmic reticulum Ca2+-ATPase (SERCA) 1 and 3 isoforms by steady-state and transient kinetic analyses. J Biol Chem 277:45579.
27. Tzeng S, Kalodimos C. (2009) Dynamic activation of an allosteric regulatory protein. Nature 462:368–372.

28. Li D-W, Showalter SA, Brüschweiler R. (2010) Entropy localization in proteins. J Phys Chem B. 114: 16036–16044.
29. Zhang Z, Sumbilla C, Lewis D, Summers S, Klein MG, Inesi G. (1995) Mutational analysis of the peptide segment linking phosphorylation and Ca(2+)-binding domains in the sarcoplasmic reticulum Ca(2+)-ATPase. J Biol Chem 270:16283–16290.
30. Mueller B, Zhao M, Negrashov I, Bennett R, Thomas D. (2004) SERCA structural dynamics induced by ATP and calcium. Biochemistry. 43:12846–12854.
31. Lenoir G, Jaxel C, Picard M, le Maire M, Champeil P, Falson P. (2006) Conformational changes in sarcoplasmic reticulum Ca 2+-ATPase mutants: effect of mutations either at Ca 2+-Binding Site II or at tryptophan 552 in the cytosolic domain. Biochemistry 45: 5261–5270.
32. Satoh K, Matsu-ura T, Enomoto M, Nakamura H, Michikawa T, Mikoshiba K. (2011) Highly cooperative dependence of sarco/endoplasmic reticulum calcium ATPase (SERCA) 2a pump activity on cytosolic calcium in living cells. J Biol Chem 286:20591–20599.
33. Rostkowski M, Olsson MH, Søndergaard CR, Jensen JH. (2011) Graphical analysis of pH-dependent properties of proteins predicted using PROPKA. BMC Struct Biol 11:6.
34. Obara K, Miyashita N, Xu C, Toyoshima L, Sugita Y, Inesi G, Toyoshima C. (2005) Structural role of countertransport revealed in Ca2+ pump crystal structure in the absence of Ca2+. Proc Nat Acad Sci 102: 14489–14496.
35. Weidemüller C, Hauser K. (2009) Ion transport and energy transduction of P-type ATPases: implications from electrostatic calculations. Biochim Biophys Acta (BBA) – Bioenerg 1787:721–729.
36. Humphrey W, Dalke A, Schulten K. (1996) VMD: visual molecular dynamics. J Mol Graphics 14:33–38.
37. Brooks BR, Brooks CL III, Mackerell AD Jr, Nilsson L, Petrella RJ, Roux B, Won Y, Archontis G, Bartels C, Boresch S, Caflisch A, Caves L, Cui Q, Dinner AR, Feig M, Fischer S, Gao J, Hodoscek M, Im W, Kuczera K, Lazaridis T, Ma J, Ovchinnikov V, Paci E, Pastor RW, Post CB, Pu JZ, Schaefer M, Tidor B, Venable RM, Woodcock HL, Wu X, Yang W, York DM, Karplus M. (2009) CHARMM: the biomolecular simulation program. J Comput Chem 30:1545–1614.
38. Phillips J, Braun R, Wang W, Gumbart J, Tajkhorshid E, Villa E, Chipot C, Skeel R, Kale L, Schulten K. (2005) Scalable molecular dynamics with NAMD. J Comput Chem 26:1781–1802.
39. Darden T, York D, Pedersen L. (1993) Particle mesh Ewald: an Nlog(N) method for Ewald sums in large systems. J Chem Phys. 98:10089–10092.
40. Wang Y, Harrison CB, Schulten K, McCammon JA. (2011) Implementation of Accelerated Molecular Dynamics in NAMD. Comput Sci Discovery. 4:015002–015012.
41. Grant BJ, Rodrigues APC, ElSawy KM, McCammon J, Caves LSD. (2006) Bio3d: an R package for the comparative analysis of protein structures. Bioinformatics 22:2695–2696.
42. Durrant J, de Oliveira C, McCammon J. (2011) POVME: an algorithm for measuring binding-pocket volumes. J Mol Graphics Modell. 29:773–776.
43. Huber GA, McCammon JA. (2010) Browndye: a software package for Brownian dynamics. Comput Phys Commun 181:1896–1905.
44. Dolinsky TJ, Czodrowski P, Li J, Nielsen JE, Jensen JH, Klebe G, Baker NA. (2007) PDB 2PQR: expanding and upgrading automated preparation of biomolecular structures for molecular simulations. Nucl Acid Res 35: W522–W525.
45. Baker NA. (2001) Electrostatics of nanosystems: application to micro-tubules and the ribosome. Proc Nat Acad Sci 98:10037–10041.
46. Northrup S, Allison S, McCammon J. (1984) Brownian dynamics simulation of diffusion-influenced bimolecular reactions. J Chem Phys 80:1517–1526.
47. Yu H, Noskov S, Roux B. (2010) Two mechanisms of ion selectivity in protein binding sites. Proc Nat Acad Sci 107:20329.